J Sol-Gel Sci Technol (2015) 74:707–717
DOI 10.1007/s10971-015-3652-1

ORIGINAL PAPER

The effect of titania precursors and ceria loadings on textural and chemical properties of TiO_2–CeO_2 and Pt–Rh/TiO_2–CeO_2

Jocelyn Miranda-Sánchez · Ignacio Elizalde · Luis Lartundo-Rojas · Isaías Hernández-Pérez · David Jaramillo-Vigueras · Román Ramírez-López

Received: 10 October 2014 / Accepted: 1 February 2015 / Published online: 14 February 2015
© Springer Science+Business Media New York 2015

Abstract The paper presents the results of the authors regarding the synthesis of TiO_2–CeO_2 mixed oxides using different precursors: (1) titanium isopropoxide and (2) titanium butoxide with different ceria loadings. The samples were characterized from chemical, structural and morphological point of view. The obtained powders were used as support for Pt–Rh impregnation and the influence the Pt–Rh in reduction of the support was established. From XPS, TPR and EPR analysis it was concluded that Ce^{3+} species are present in higher proportion (>50 %) in series supported Pt–Rh catalysts and it was taken as indicative of oxygen mobility. Correlation between ceria loading and percentage of Ce^{3+} in catalytic samples was observed. It was also evident that Rh addition allows increasing the reducibility of materials due to interactions metal-support.
Graphical Abstract

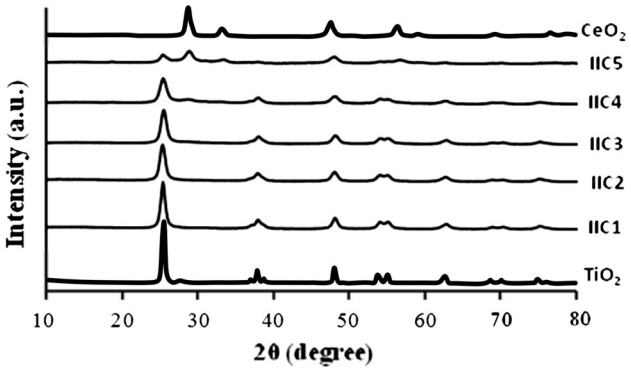

Keywords Titania precursor · Ceria loading · TiO_2–CeO_2 · Rh-ceria interaction

1 Introduction

Cerium oxide is a compound that has been used in the development of materials for diverse purposes including the abatement of vehicle emissions, fluid catalytic cracking, fuel cells, removal of organics from wastewater and photocatalysis [1, 2]. The wide use of such a rare earth is due to its ability to promote and improve the activity, selectivity and thermal stability of catalysts [1]. These behaviors are related mainly to its high capacity to store/release oxygen (oxygen storage capacity—OSC) and to its low redox potential to pass from C^{4+} to Ce^{3+} [3]. The main disadvantages are that it cannot be used as catalyst alone due to low stability under reaction conditions and its very low surface area [1–3].

Titania on the other hand, has been subject of major attention due to chemical stability, low cost and non-toxicity. Its uses include biomaterials, catalyst support and

J. Miranda-Sánchez · D. Jaramillo-Vigueras
Centro de Investigación e Innovación Tecnológica (CIITEC-IPN), 02250 Mexico, D.F., Mexico

J. Miranda-Sánchez · I. Hernández-Pérez · R. Ramírez-López
Escuela Superior de Ingeniería Química e Industrias Extractivas (ESIQIE-IPN), 07738 Mexico, D.F., Mexico

I. Elizalde (✉)
Centro Mexicano para la Producción más Limpia (CMPL-IPN), Instituto Politécnico Nacional, Ticomán, 07340 Mexico, D.F., Mexico
e-mail: ielizaldem@gmail.com

L. Lartundo-Rojas
Centro de Nanociencias y Micro y Nanotecnologías (CNMN-IPN), 07738 Mexico, D.F., Mexico

additive in catalytic reactions and also in photocatalysis, this last application related with titania anatase phase [4–10]. The main disadvantage of pure anatase is its limitation as photocatalyst by using as source the solar energy.

Mixing oxides allows for creating in some cases a synergetic effect between them [3, 11]. In the case of titania-ceria mixed oxides they allow for obtaining a TiO_2 sensible to solar energy or to improve the thermostability of CeO_2 at high temperatures among other applications. For example TiO_2–CeO_2 has been used as support for Pt catalyst favoring the isomerisation and hydrogenolysis reactions of 2- and 3-methylpentanes, *n*-hexane and methylcyclopentane [12] and dehydration of methanol to formaldehyde at low temperature [13].

Sol–gel technique in one of the most preferred technique to synthesize catalysts due to high homogeneity of prepared materials and the possibility of controlling the structure of products [14]. There is evidence that TiO_2–CeO_2 mixed oxides can promote the segregation and sintering of disperse crystals of CeO_2 on the surface of TiO_2 granules after thermal treatment, and insert Ce^{4+} ions within TiO_2 network or insert Ti^{4+} ions in CeO_2 network by the same cause [15]. At low proportion of Ti^{4+} in TiO_2 lattice substitution by Ce^{4+} is achieved [16] under specific conditions. Another feature that exhibits the mixed support is the grade of sintering of TiO_2 that is diminished by the presence of ceria in the range of temperatures of 473–873 K [17, 18].

Depending on ceria loading it has been observed that TiO_2–CeO_2 can exhibit different behavior [19]. For example Watanabe et al. [20] have found that surface of TiO_2–CeO_2 mixed oxide changes as ceria content does. Watanabe et al. [20] also have found a minimum of surface area between different mixed oxides when proportion between Ti and Ce was 0.3:0.7. As titania proportion was increased so did surface area. They found that surface area of ceria-titania mixed oxides ranges between surface areas of pure ceria and titania. Another important feature of the same study was that increasing titanium content in mixed oxide an increase of reduction temperature was observed. In another study Milenova et al. [21] have observed that depending on ceria and titania proportion the photocatalytic activity toward Reactive Black 5 under UV-light illumination was also different.

Due the characteristics of ceria, adding precious metal enables it to form intermetallic Ce-M phase faciliting the reduction of supported noble metals [2, 22]. It is found that independently of the second oxide in ceria mixed oxides redox property changes significantly with addition of noble metals which in turn perform different as the concentration of such metal change due to the so called the *SMSI* effect (Strong Metal-Support Interactions). It has been reported in previous research [23] the significant improvement on TiO_2–CeO_2 mixed oxide with addition of trace amounts of Rh (0.005 wt%) and it was also concluded that the presence of Rh strongly facilitates the reducibility of ceria in TiO_2–CeO_2 mixed support. The presence of ceria can contribute to maintain high dispersion of precious metals and thus synergetic effect is generated between precious metal and rare earth.

The effect of titania precursor on ceria-titania mixed supports has not been evidenced up until now. Different titania precursors have been employed for different purposes, for example: titanium isopropoxide [11, 19, 24–27], $TiCl_4$ [15], titanium 2-methyl-2-butoxide [17], titanium oxysulfate [20], aqueous titanyl acetylacetonate [23], titanium butoxide [18, 28] among others. The combination of several other factors during titania-ceria synthesis such as calcination temperature, the use of surfactants and the method of preparation does not permit recognize the influence of titania precursor on physical and chemical properties of mixed oxide.

From the above introduction it is clear that multiple variables affect the behavior of mixed oxides supported precious metals and unique features are exhibited for each particular synthesis and ulterior treatment.

In this contribution we explore the effect of two different titania precursors and ceria loading on physical and chemical properties of TiO_2–CeO_2 mixed oxides and TiO_2–CeO_2 supported Pt–Rh catalysts by using several techniques of characterization. Some relevant findings are reported below.

2 Experimental

2.1 Synthesis of materials

Titania and TiO_2–CeO_2 mixed oxides were synthesized by sol–gel method by using cerium (III) nitrate hexahydrate (Aldrich, 99.9 %), nitric acid (JT Baker, 69.9 %) and two titania precursors: (a) For first series labeled as IICx, titanium isopropoxide (Aldrich, 97 %) and isopropyl alcohol (JT Baker, 99.9 %) were used, and (b) for second series labeled as BECx, titanium butoxide (Aldrich, 97 %) and ethylic absolute alcohol (JT Baker, 99.9 %) were employed. Both series of mixed supports with different ceria concentrations were prepared.

Molar ratio of alcoxide/alcohol, alcoxide/water, and alcoxide/nitric acid were 60, 20 and 0.05 respectively. Firstly $Ce(NO_3)_3{\cdot}6H_2O$ was dissolved in alcohol. On the other hand a mixture of distillate water, alcohol and nitric acid was prepared. After that these two solutions were mixed at constant ambient temperature and pH by stirring vigorously. The products were dried at 100 °C by 24 h. Then the samples were calcined according with TGA analysis at 600 °C.

The addition of Pt and Rh to supports was carried out by incipient wetness impregnation with rhodium (III) chloride hydrate (Aldrich, 38 %) and hexachloroplatinic acid (Aldrich, 99 %). The catalysts were obtained by calcining the samples at 600 °C for 4 h.

2.2 Characterization of supports

2.2.1 Termogravimetric analysis

Thermogravimetric analysis (TGA) and derivative thermogravimetric analysis (DTG) were carried out by using a thermogravimetric analyzer SDT Q 600 V20.9 build 20 Module DSC–TGA Standard. Samples were heated up to 800 °C at 10 °C/min in presence of nitrogen flow.

2.2.2 Textural properties (BET)

The surface area, pore volume and pore size distribution of calcined solid samples were measured by nitrogen adsorption at 77.4 K with ASAP 2020 (Micromeritics Instrument Co. USA). The samples were degassed at 150 °C and 80.377 kPa for 22 h prior to adsoption/desorption measurements.

2.2.3 X-ray diffraction analysis (XRD)

The crystalline structure of samples was identified by X-ray diffraction by using a Rigaku miniflex 600 diffraction spectrometer. The diffraction patterns were recorded over a 2θ range of 10°–80° at a scanning speed of 3°/min and room temperature using Cu-Kα radiation (1.5417 Å), 40 kV and 15 mA.

2.3 Characterization of catalysts

2.3.1 Chemical composition

The chemical composition of the catalysts was determined by inductively coupled plasma (ICP) atomic emission spectroscopy with a Perkin Elmer Optical Emission Spectrometer Optima 2100 DV system.

2.3.2 Temperature-programmed reduction (TPR)

Temperature-programmed reduction (TPR) analysis was carried out by an in-house apparatus. About 50 mg the powder sample was loaded in a U-shaped quartz cell. The TPR profile of the samples was recorded between room temperature and 600 °C at a heating rate of 10 °C/min in 10 % H_2 using argon as carrier with flowrate of 100 mL/min. Hydrogen uptake was monitored by a TCD detector.

2.3.3 X-ray photoelectron spectroscopy (XPS)

The X-ray photoelectron spectra were obtained with a Thermo Scientific K-Alpha system with a monochromatic Al Kα source (1487 eV) with analysis area of 400 μm. The analysis chamber pressure was 10^{-9} mBar. The binding energies were determined by utilizing O1s line as a reference (531.0 eV). From high resolution spectra, a quantitative analysis was performed out averaging three points at different surface zones. Peak fitting was done with Shirley background and Lorentzian:Gaussian deconvolution shapes were used.

2.3.4 Electron paramagnetic resonance (EPR) spectroscopy

X-band EPR spectra were collected using an EMX Plus Bruker System, with an ER 041 XG microwave bridge and an ER 4102ST cavity. The following conditions were used: microwave power of 10 mW; modulation amplitude of 5 G; modulation frequency of 100 kHz; time constant of 327 ms; conversion time of 82 ms; and averaging over 12 scans.

3 Results and discussion

3.1 Prepared powders

3.1.1 Thermogravimetry

TGA and DTG for uncalcined hydrolysis products from both titania precursors and 8 wt% theoretical Ce loading are shown in Figs. 1 and 2, respectively. For the sample IIC3 (Fig. 1) a weight loss of ca 22 wt% was recorded from room temperature to 800 °C while for sample BEC3

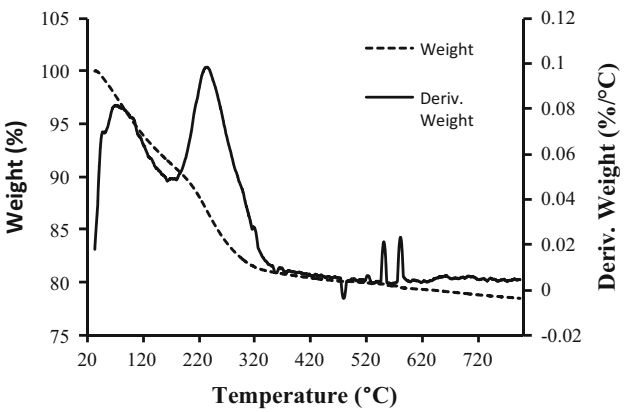

Fig. 1 TGA and DTG curves of uncalcined hydrolysis products: IIC3 sample

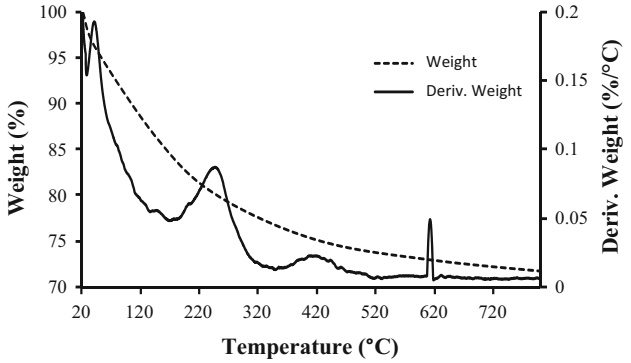

Fig. 2 TGA and DTG curves of the uncalcined hydrolysis products: BEC3 sample

(Fig. 2) a weight loss of about 28 wt% was observed under the same range of temperatures.

For the IIC3 sample at ca 72.5 °C desorption of water occurs while the change at approximately 235 °C was related with OH evolution. Peak at 580 °C could be assigned to Ce^{3+} to Ce^{4+} oxidation. For the BEC3 sample a signal at 42 °C is also attributed to dehydration of powders, while a peak at 247.3 °C was assigned to the structural evolution of OH. Finally the signal at 613 °C was related to Ce^{3+} to Ce^{4+} oxidation.

In all cases the loss weight between 600 and 800 °C was very small, which ensures the almost complete removal of volatiles at 600 °C and no further increase in calcination temperature is necessary. This finding is in agreement with other reports [27].

Broadly speaking, it was found that samples of the first and second series exhibits similar behavior among them. However, materials of IIC have exhibited more variation in weight loss than those of BEC.

3.1.2 Nitrogen gas adsorption

In Figs. 3a, b and 4a, b N_2 adsorption–desorption isotherms for IIC and BEC systems are shown. Both series exhibits isotherms type IV, according to IUPAC classification [29]. These isotherms are typical of mesoporous materials (pore size between 2 and 50 nm), a characteristic of a material synthesized by the sol–gel method similar to that reported in a previous study [27]. The hysteresis loop of type H2 can be observed in the pores with narrow necks and wider bodies (ink-bottle pores). Average pore diameter, specific surface area and pore volume were determined from BET analysis.

In Table 1 the surface area, pore volume and average pore diameter of samples for IIC and BEC are reported. It is observed a maximum surface area in sample IIC3, while pore volume was the largest for samples IIC3 and IIC4, this maximum remained stable at these range of ceria

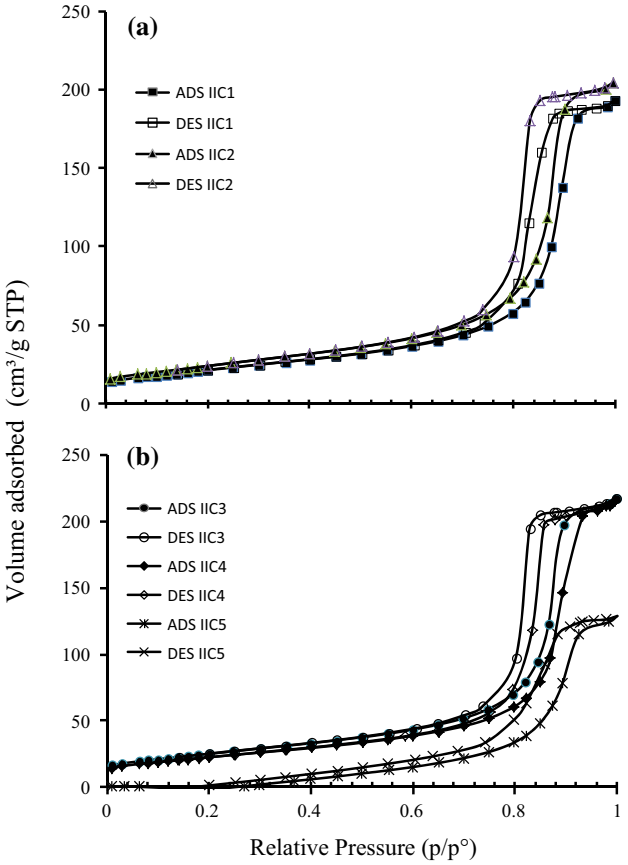

Fig. 3 N_2 Adsorption/desorption isotherms for calcined IICx samples

concentration. Considering the average pore diameter it is shown that samples exhibits the following behavior (except IIC1): as ceria loading increases so does the diameter size, being IIC5 the sample with the highest average pore diameter.

For samples from BEC also surface area showed a maximum at 8 wt% of the theoretical ceria loading, which is similar for IIC. This could be attributed to a better arrangement of atoms of Ti and Ce at that concentration. The sample BEC3 had the maximum of pore volume (0.18 cm^3/g) but for the case of average pore diameter the maximum value was represented in sample BEC1 with 16.0 nm. In contrast with IIC samples, no appreciable effects on average pore diameter were observed in BEC samples by changing ceria concentration in the support.

Pore size distribution for IIC and BEC systems are shown in Fig. 5a, b respectively. A narrow unimodal distribution was shown for all samples. IIC system pore distribution ranged between 8 and 17 nm with IIC5 sample showing the broadest pore distribution among samples of IIC.

Pore size distribution for BEC samples varied between 4 and 20 nm. It is shown that BEC3 sample exhibited

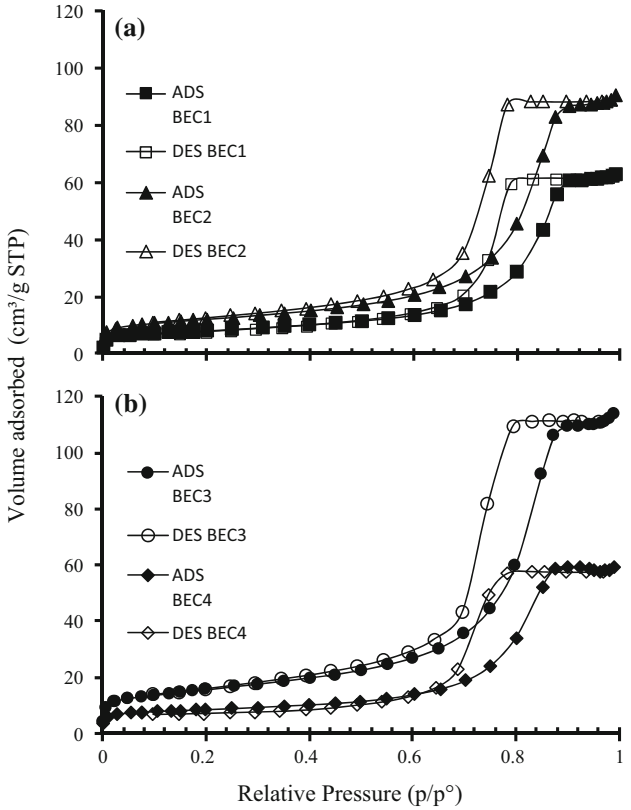

Fig. 4 N_2 Adsorption/desorption isotherms for calcined BECx samples

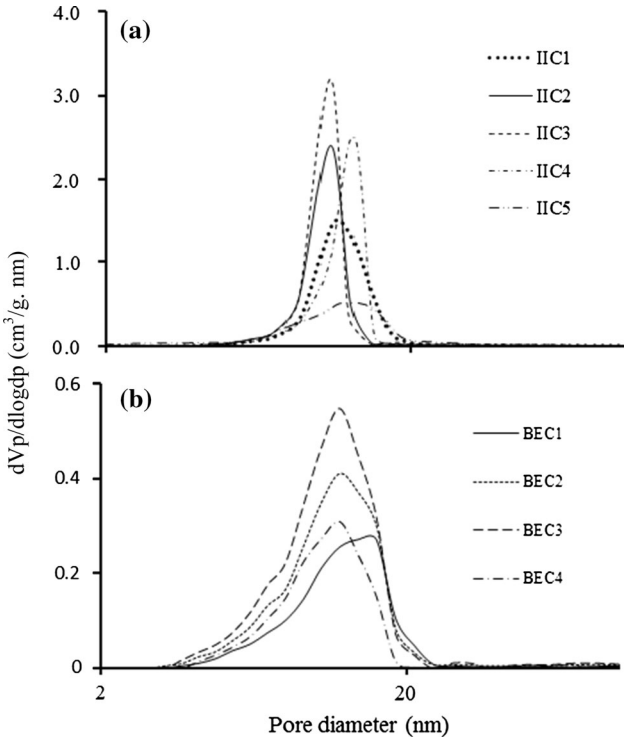

Fig. 5 Pore size distribution of calcined samples

Table 1 Textural properties of TiO_2–CeO_2 mixed supports

	Surface area (m^2/g)	Pore volume (cm^3/g)	Average pore diameter (nm)
IIC			
1	76.5	0.30	15.1
2	86.3	0.31	14.4
3	90.7	0.33	14.5
4	81.1	0.33	16.2
5	42.9	0.20	17.9
BEC			
1	27.4	0.10	16.0
2	41.9	0.14	12.1
3	53.9	0.18	12.1
4	30.0	0.09	12.1

broadest pore distribution among samples having the BEC1 sample the narrowest distribution.

Comparing textural properties of IIC and BEC it is observed that surface area, pore volume and pore diameter were higher in samples of IIC system than in samples of BEC system. Regarding to pore size distribution, BEC system exhibited broader distribution than IIC system. All these behaviors can be attributed to titania precursors, that is, textural properties are favored by using titanium isopropoxide precursor over titanium butoxide. Hence it can be summarized that the first precursor favors the formation of more porous structure during the crystal growing process as it has been observed in previous study [20].

3.1.3 X-ray diffraction

Figures 6 and 7 show the XRD spectra of mixed oxides of the systems IIC and BEC, respectively. Ceria and titania spectra have been included in both figures for reference.

In both series the more visible peaks were those corresponding to titania and they were located at diffraction lines of $2\theta = 25.5$, 38, 48.2, 54, 55.3, 62.9 and 68.9° which coincides with anatase phase.

Ceria-titania mixed oxides displayed XRD patterns that correspond to titania anatase phase. The peaks of different samples become weaker as ceria loading increase which is in agreement with previous reports [28, 30].

Additionally reflections peaks due to cubic fluorite CeO_2 corresponded to diffraction lines at $2\theta = 28.8$, 33.4, 56.7 and 59.3°. These peaks were evident for sample with the highest ceria content (IIC5).

BEC system presented a similar behavior as IIC. The presence of cerianite crystal was not determined. Again, the higher the ceria content, the weaker the peak intensity, that means that titania anatase phase in the mixed oxide

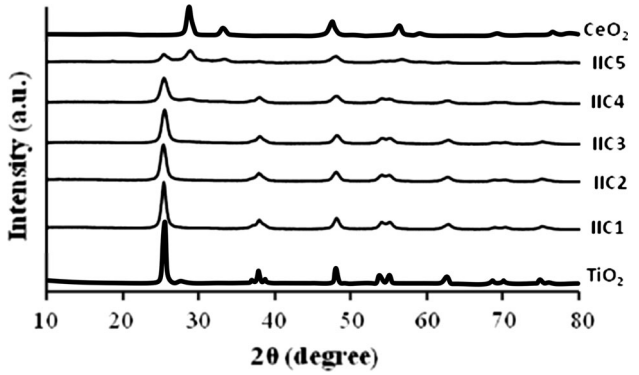

Fig. 6 XRD diffraction patterns for IICx samples and pure CeO_2 and TiO_2

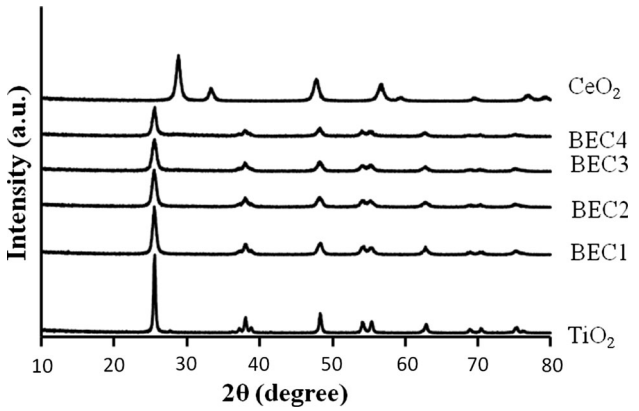

Fig. 7 XRD diffraction patterns for BECx samples and pure CeO_2 and TiO_2

depends mainly on ceria concentration and not directly on the titania precursor.

The average crystallite sizes of TiO_2 anatase and cubic fluorite CeO_2 in the mixed oxide were calculated from Debye–Scherrer equation using the plane (1 0 1) diffraction peak of anatase at 25.4° and the plane (1 1 1) diffraction peak of the cubic fluorite CeO_2 at 28.8°. The crystallite size of the CeO_2 and TiO_2 were 16 nm and 33 nm, respectively. For the samples IICx and BECx the results are shown in Table 2. It was observed a correspondence between ceria loading and anatase crystal size for System I as ceria concentration increases, the size of titania crystal diminishes, ceria deteriorates the crystallinity of titania anatase phase in the mixed oxide provoking the reduction of the crystal size as reported previously [24, 31]. In BEC system, titania anatase did not exhibit a correspondence between crystal size and ceria concentration. Different interaction between titania and ceria in mixed oxides can be expected in the last case and such behavior could be attributed to the titania precursor.

Table 2 Crystal size of titania anatase phase and ceria in mixed oxides

Sample	2θ(°)	Anatase, cristal size (nm)	2θ(°)	Cerianite, cristal size (nm)
IIC				
1	25.4	13	–	–
2	25.3	11	–	–
3	25.5	10	–	–
4	25.4	8	–	–
5	25.3	6	28.8	6
BEC				
1	25.5	14	–	6
2	25.47	13	–	–
3	25.49	13	–	–
4	25.5	16	–	–
TiO_2	25.5	33	–	–
CeO_2	–	–	28.8	16

No crystalline phases were detected corresponding to Ce–Ti–O oxides which was attributed to the method of synthesis and low calcination temperature used in our experiments.

From the above results, it is evident that ceria had influence on anatase crystal size and it is more evident in samples of IIC than in samples of BEC. In addition BEC samples had an inverse effect of ceria loading in anatase crystal size when they are compared with samples of IIC.

Comparing all the obtained data it can be observed that titania precursor can limit the formation and grow of ceria crystals. The mechanism by which it occurs has not been elucidated.

3.1.4 H_2-TPR of mixed supports

Figure 8a shows the hydrogen uptake as function of temperature for IICx catalyst (TPR of ceria alone is shown for reference). TPR of titania was not included because it did not exhibit any change during TPR experiment which is in agreement with previous reports [20]. Ceria in pure form exhibits a shoulder between 400 and 500 °C and a peak at ca. 530 °C that is attributed to the surface oxygen removing [22].

It was observed that as ceria loading increases in mixed oxides so does the oxygen mobility. This fact has been observed by others [20]. Such behavior can be attributed to ceria that allows release oxygen easily at high concentrations as a consequence of the exposed surface and defect structures. Meanwhile, at low ceria loading the ceria species can be trapped in the oxide network limiting the oxygen mobility and hence its degree of reduction. At

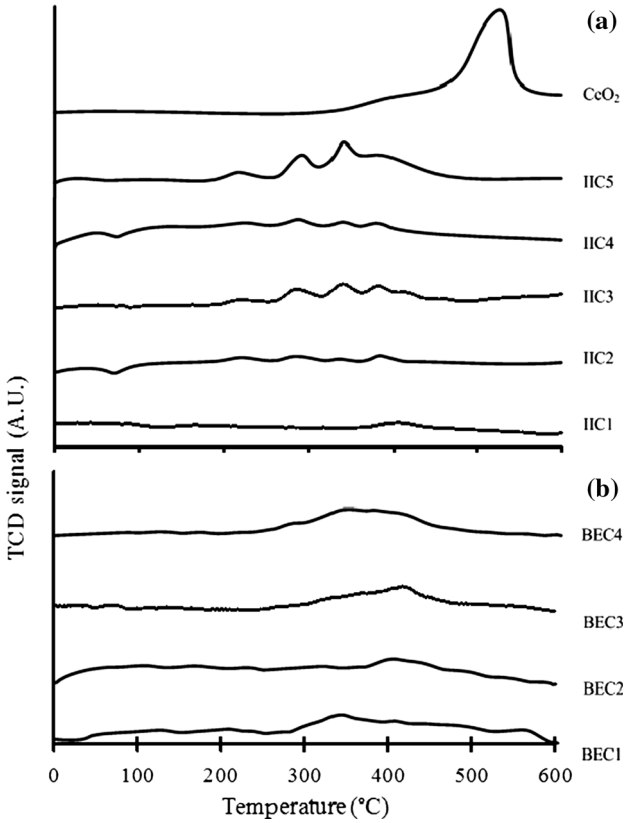

Fig. 8 H_2-TRP profiles of pure ceria and synthesized mixed supports

218 °C samples IIC4-5 exhibited a shoulder, while at 289, 340 and 390 °C peaks were identified. However at higher temperatures, there was no evidence of peaks. For sample IIC2 peaks at 289 and 340 °C were observed while sample IIC1 a weak peak at 410 °C is exhibited. It is established that peaks below 400 °C can be related to the reduction of surface oxygen [32] and above this temperature the peaks are attributed to material bulk reduction. Hence materials of IIC only exhibited reduction of ceria at the material surface. Probably titania inhibited the oxygen mobility of ceria because interaction between mixed oxides.

H_2-TPR for BEC is presented in Fig. 8b. Weak signals at 346 °C (BEC1), 363 °C (BEC4) and 423 °C (BEC2, BEC3) are shown, which again can be attributed to surface ceria reduction. Oxygen mobility increased with ceria loading but compared with IIC, mixed oxides of BEC exhibited lower ability to release oxygen. One factor that can contribute to this behavior is their low surface area that could limit the OSC capacity [33]. It seems that materials of BEC system are more heterogeneous than IIC system because they do not exhibit any correlation between ceria loading and TPR signal at the same temperatures. Also the effect of titania precursor may play an important role because it limits the OSC capacity for BEC samples and favors the oxygen mobility for IIC.

Table 3 Chemical composition of catalysts

	wt%		
	Ce	Pt	Rh
Pt–Rh/IIC			
1	1.36	0.11	0.11
2	3.70	0.11	0.12
3	7.24	0.11	0.12
4	14.60	0.11	0.11
5	37.47	0.10	0.11
Pt–Rh/BEC			
1	1.29	0.11	0.12
2	3.31	0.10	0.12
3	7.42	0.11	0.11
4	12.03	0.10	0.11

3.2 Pt–Rh doped powders

3.2.1 ICP of Pt–Rh/mixed-oxides

After impregnation of TiO_2–CeO_2 mixed supports of both series with Pt and Rh their composition was determined and presented in Table 3. Differences between theoretical and actual composition can be attributed to washing out of some materials during preparation.

3.2.2 X-ray photoelectron of Pt–Rh/mixed-oxides

To investigate the species of ceria on the catalyst surface an automatic Lorentzian-Gaussian deconvolution *XPS* spectra of catalytic samples were performed. *XPS* spectrum Pt–Rh/IIC3 and Pt–Rh/BEC3 samples are presented in Fig. 9a, b. For others Pt–Rh/IIC similar behavior was found, but figures were not included.

By using deconvolution of XPS spectra information of the percentage of Ce^{3+}/Ce^{4+} for samples of IIC and BEC was determined. The Ce 3_d spectrum of the catalysts denotes a mixture of Ce^{3+}/Ce^{4+} oxidation states. Table 4 shows the percentage of Ce^{3+} calculated for catalysts. The labels used in the identification of Ce 3_d XPS were established by Burroughs et al. [34], where *v* and *u* indicate the spin–orbit coupling $3d_{5/2}$ and $3d_{3/2}$, respectively. The existence of the Ce^{3+} was attributed to the interaction between ceria and the surrounding atoms which Li et al. [35] used as indicator for the existence of oxygen vacancies.

The main $3d_{5/2}$ features were at 882.7, 888.8 and 898.7 eV and $3d_{3/2}$ at 901, 906.8 and 916.9 eV of pure ceria are observed in all samples of both supported series catalysts. New bands at ca. 880, 885 and 903 appeared. The new peaks could give evidence of different configuration

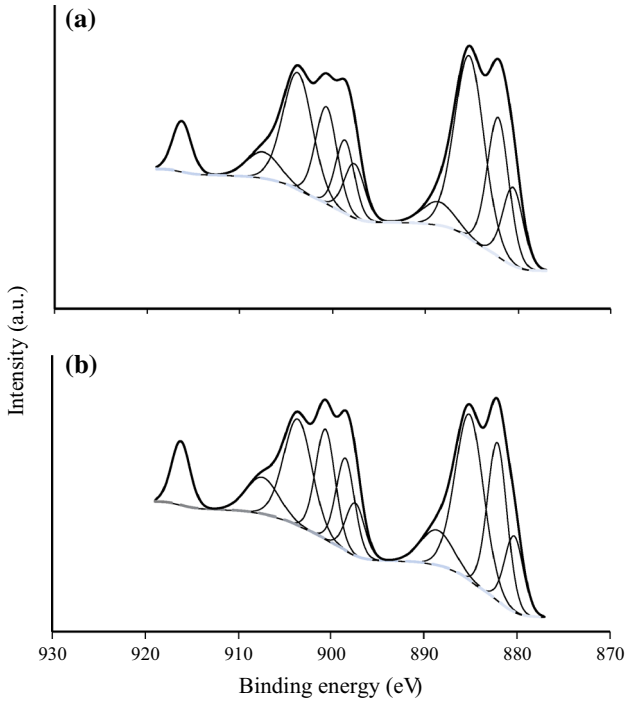

Fig. 9 The XPS spectrum of Ce 3_d for Pt–Rh/IIC3 and Pt–Rh/BEC3

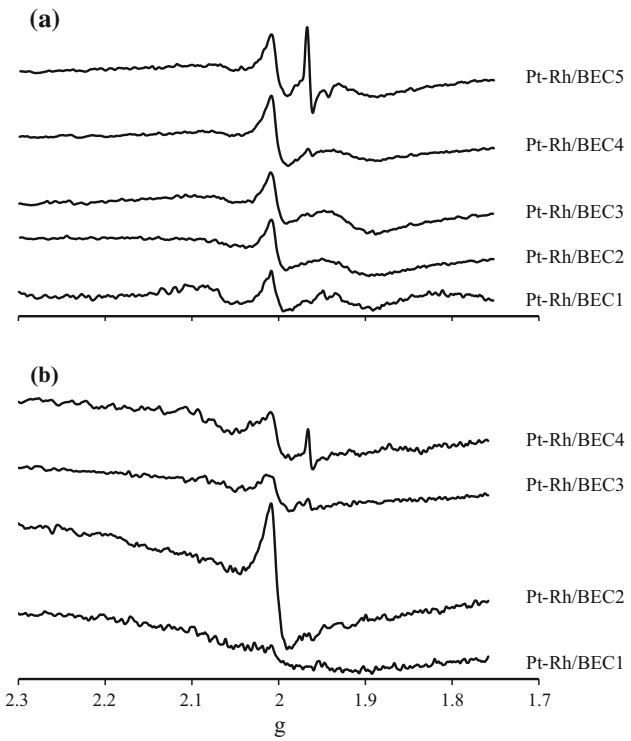

Fig. 10 EPR spectra of catalytic samples

Table 4 Percentages of Ce^{3+} and Ce^{4+} in Pt–Rh/TiO_2–CeO_2 samples determined from XPS analysis

	Ce^{3+}	Ce^{4+}
Pt–Rh/IIC		
1	71	29
2	63	37
3	58	42
4	56	44
5	51	49
P–Rh/BEC		
1	42	58
2	58	42
3	48	52
4	44	56

states and non-stoichiometric ceria at the surface of titania-ceria mixed oxides.

There is evidence that sol–gel method allows reach high Ce^{3+} percentages (higher than 50 %) in TiO_2–CeO_2 samples as it was confirmed in this study [11]. The percentage of Ce^{3+} for Pt–Rh/IICx samples exhibited some correlation with ceria loading: As ceria loading increases, the Ce^{3+} percentage decreased in a negative exponential fashion. A factor that can contribute to this behavior is the facility of reoxidation of the nonstoichiometric ceria at ambient conditions and some interactions of ceria with titania.

A relative low sensibility to ceria loading is shown for Pt–Rh/BECx samples respect to Ce^{3+} content. Ceria crystals could be plugging the material pores as was evidenced by the low surface area and then it could provoke low exposition of Ce^{3+}.

3.2.3 EPR of Pt–Rh/mixed-oxides

Figure 10a exhibits the EPR spectra of IIC supported Pt–Rh catalysts. Different signal intensity was observed, the weaker intensity corresponds to those with lower ceria content. The first signal g = 1.96 corresponds to a unique ceria signal and it is attributed to impurities [36, 37]. The second signal at $g = 2.05$ is attributed to the presence of Ce^{3+} which corresponds to oxygen vacancies [37]. It has been stated that such vacancies may trap electrons that generate those signal [37]. Also it has been proposed that Ce^{3+} species may contribute to the resonance line at $g = 2.05$. This observation agrees with XPS measurements in which it was determined that more than 50 % of cerium species correspond to that state for samples of Pt–Rh/IICx.

For BEC supported Pt–Rh catalysts similar g values ($g = 1.96$ and 2.05) were exhibited in Fig. 10b but now signal intensity is not proportional to ceria loading being the strongest for sample with 3.31 wt% ceria. According to XPS analysis this catalytic sample (Pt–Rh/BEC2) has the highest Ce^{3+} percentage and this may be a reason of the intensity of the EPR signal. Another feature that exhibits materials of BEC supported Pt–Rh catalysts are that EPR

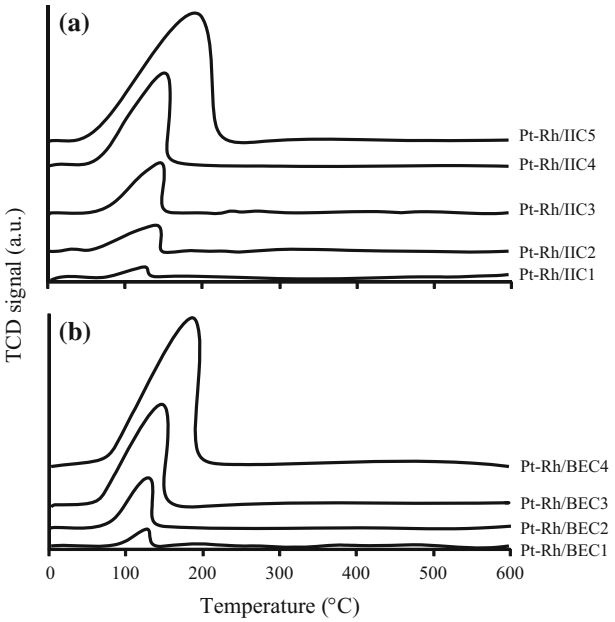

Fig. 11 H_2-TRP profiles of synthesized catalysts

spectra are distorted which could be attributed to unhomogeneities of such samples.

Comparing EPR results for the two series of catalysts it can be concluded that they exhibited signals at the same positions and these correlate well with XPS analysis. However it was observed no uniformity of samples of BEC compared with IIC supported Pt–Rh catalysts due to the effect of titania precursor.

3.2.4 H_2-TPR of Pt–Rh/mixed-oxides

In Fig. 11a H_2-TPR profiles of Pt–Rh/IICx were depicted. A unique peak was observed for each sample. These peaks exhibited different behaviors depending on ceria loading. As ceria concentration was risen, they were an increment of the signal intensity (hydrogen consumption), the broad the peak and increase the reduction temperature. This peak could be attributed to reduction of Rh species in the metal-support interface as it has been previously reported [38–40]. A stronger interaction between Rh and ceria surface was favored as ceria loading grew that in turn allowed a higher remotion of oxygen but also required more energy to activate the oxygen mobility, in agreement with literature report [41]. No evidence of peak related to the reduction of platinum or rhodium oxides at crystal surface was found perhaps because the low concentration of precious metals.

The center of Pt–Rh/BECx catalysts peaks was located between 120 and 183 °C as it can be seen in Fig. 11b. The behavior was similar to Pt–Rh/IIC catalysts. Pt–Rh/BEC1-3 sample had a similar reduction temperature as Pt–Rh/IIC1-3 samples which can be attributed to similarity in ceria composition attributing to the slightly differences of titania precursor. Significant difference existed between Pt–Rh/BEC4 and Pt–Rh/IIC4 catalysts which could be related to the difference on ceria concentration (12 against 14.5 wt%). Part of this behavior can be attributed to the precious metals as a consequence to the similar concentration in both systems. Also the presence of platinum seems not to influence the behavior of the materials; at least this effect was not appreciable, probably due to low interaction with ceria and low concentration.

4 Final remarks

In general it can be outlined that reduction of materials of the two series of catalysts depends slightly on titania precursor at our experimental conditions. It would be of interest to perform tests at other percentages of ceria loadings in order to support our preliminary conclusion. It is demonstrated the existence of Ce^{3+} and Ce^{4+} species at the material surface being an indicative of oxygen vacancies as it can be proved from XPS to EPR measurements.

It was also found that ceria loading in catalytic samples correlates with textural properties in some fashion. In the case of mean pore diameter and pore volume depending on precursor such a relation is different. The mobility of oxygen in mixed supports depends more on titania precursors because when using titanium isopropoxide such behavior almost was proportional to ceria loading but by using titanium butoxide there was no correlation. Adding low amounts of Rh to TiO_2–CeO_2 supports allowed to improve the OSC capacity due to SMSI effect, but addition of Pt do not affect the OSC capacity without any dependence on titania precursor. More research on the effect of titania precursor need to be carried out in order to investigate the role of such reagent in the physical and chemical properties of TiO_2–CeO_2 mixed oxides.

5 Conclusions

Two precursors of titania (titanium isopropoxide and titanium butoxide) were used in the synthesis of titania-ceria mixed oxide by sol gel method with different ceria loadings. These mixed oxides exhibited different behaviors depending on titania precursor. It was found that by using titanium isopropoxide, there were larger surface areas and better oxygen mobility. Also a correlation between titania crystal size and ceria loading was found. On the contrary, samples with titanium butoxide precursor exhibited no direct correlation between ceria loading, textural properties and titania anatase crystal size.

After impregnation of titania-ceria mixed oxides with Pt–Rh it was found that reduction of the support occurred at lower temperatures that those corresponding to the supports alone. This was attributed to interactions between Rh and ceria. Samples whose precursor was titanium isopropoxide exhibited a good correlation between reduction temperature and Ce^{3+} percentage with ceria loading while samples synthesized from titanium butoxide did not exhibit such a relation.

Acknowledgments We thank MSc Esau E Rodrígez, Centro de Investigación y de Estudios Avanzados-IPN, for EPR measurements. Facilities during mixed supports synthesis and H_2-TPR measurements of mixed oxides provided by Dr. Carmen Reza, ESIQIE, and Dr. Tomás Viveros, Universidad Autónoma Metropolitana (UAM-I), respectively are greatly acknowledged. J. Miranda-Sánchez thanks CONACyT-México by doctoral fellowship at CIITEC-IPN. We also thank Dr. Mauricio Ángeles and Dr. Fernando Trejo for proofreading the manuscript.

References

1. Trovarelli A, Leitenburg C, Boaro M, Dolcetti G (1999) The utilization of ceria in industrial catalysis. Catal Today 50:353–367
2. Trovarelli A (ed) (2002). Catalysis by ceria and related materials. Catalytic science series. V2. Imperial College Press, London
3. Trovarelli A, Boaro M, Rocchini E, Leitenburg C, Dolcetti G (2001) Some recent developments in the characterization of ceria-based catalysts. J Alloy Comp 323–324:584–591
4. Kasemo B, Lausmaa J (1986) Surface science aspects on inorganic biomaterials. Crit Rev Biocompat 2:335–380
5. Tanaka K, Capule MFV, Hisanaga T (1991) Effect of crystallinity of TiO_2 on its photocatalytic action. Chem Phys Lett 187(1–2): 73–76
6. Karakitsou KE, Verykios XE (1993) Effects of altervalent cation doping of TiO_2 on its performance as a photocatalyst for water cleavage. J Phys Chem 97:1184–1189
7. Linsebigler AL, Lu G, Yates JT (1995) Photocatalysis on TiO_2 surfaces: principles, mechanisms, and selected results. Chem Rev 95(3):735–758
8. Hadjiivanov KI, Klissurski DG (1996) Surface chemistry of titania (anatase) and titania-supported catalysts. Chem Soc Rev 25:61–69
9. Kholmanov IN, Barborini E, Vinati S, Piseri P, Podestà A, Ducati C, Lenardi C, Milani P (2003) The influence of the precursor clusters on the structural and morphological evolution of nanostructured TiO_2 under thermal annealing. Nanotechnology 14: 1168–1173
10. Carp O, Huisman CL, Reller A (2004) Photoinduced reactivity of titanium dioxide. Prog Solid Stat Chem 32:33–177
11. Rynkowski J, Farbotko J, Touroude R, Hilaire L (2000) Redox behaviour of ceria–titania mixed oides. Appl Catal A 203: 335–348
12. Dauscher A, Maire G (1991) Isomerisation and hydrogenolysis reactions of hexanes over platinum catalysts supported on physical mixtures of TiO_2 and CeO_2. J Mol Catal 69(2):259–270
13. Agnoli S, Reeder AE, Senanayake SD, Hrbek J, Rodriguez JA (2014) Structure and special chemical reactivity of interface-stabilized cerium oxide nanolayers on TiO_2 (110). Nanoscale 6:800–810
14. Lee J, Gouma PI (2012) Chapter 11. Sol-gel processed oxide photocatalysts. In: Aparicio M, Jitianu A, Klein LC (eds) Sol-gel processing for conventional and alternative energy. Springer, New York
15. Reddy BM, Khan A, Yamada Y, Kobayashi T, Loridant S, Volta JC (2003) Structural characterization of CeO_2–TiO_2 and V_2O_5/CeO_2–TiO_2 catalysts by Raman and XPS techniques. J Phys Chem B 107:5162–5167
16. Huheey JE (1978) Inorganic chemistry. Harper & Row, New York
17. Koebrugge GW, Winnubst L, Burggraaf AJ (1993) Thermal stability of nanostructured titania and titania-ceria ceramic powders prepared by the sol-gel process. J Matter Chem. 3(11): 1095–1100
18. Lopez T, Rojas F, Alexander-Katz R, Galindo F, Balankin A, Buljan A (2004) Porosity, structural and fractal study of sol-gel TiO_2–CeO_2 mixed oxides. J Solid Stat Chem 177:1873–1885
19. Zaharescu M, Wittmar A, Teodorescu V, Andronescu C, Wittmar M, Veith M (2009) TiO_2-CeO_2 nanometric powders prepared by sol-gel method. Z Anorg Allg Chem 635:1915–1924
20. Watanabe S, Ma X, Song C (2009) Characterization of structural and surface properties of nanocrystalline TiO_2–CeO_2 mixed oxides by XRD, XPS, TPR, and TPD. J Phys Chem C 113: 14249–14257
21. Milenova K, Zaharieva K, Cherkezova-Zheleva Z, Kunev B, Blaskov V, Stambolova I, Mitov I (2014) Photodiscoloration of reactive black 5 dye using mechanochemically activated TiO_2–CeO_2 photocatalysts. Mater Methods Technol 8:241–249
22. Damyanova S, Bueno JMC (2003) Effect of CeO_2 loading on the surface and catalytic behaviors of CeO_2–Al_2O_3–supported Pt catalysts. Appl Catal A 253:135–150
23. Berger-Karin C, Wohlrab S, Rodemerck U, Kondratenko EV (2012) The tremendous effect of trace amounts of Rh on redox and catalytic properties of CeO_2–TiO_2 and Al_2O_3 in CH_4 partial oxidation. Catal Commun 18:121–125
24. Shi ZM, Yu WG, Bayar X (2004) Study of crystallization behavior of Ce^{4+}-modified titania gels. Scr Mater 50:885–889
25. Zhou G, Hanson J, Gorte RJ (2008) A thermodynamic investigation of the redox properties of ceria-titania mixed oxides. Appl Catal A 335:153–158
26. Sun DL, Heusing S, Puetz J, Aegerter MA (2003) Influence of water on the electrochemical properties of $(CeO_2)_x(TiO_2)_{1-x}$ and WO3 sol–gel coatings and electrochromic devices. Solid Stat Ion 165:181–189
27. Sinha AK, Suzuki K (2005) Preparation and characterization of novel mesoporous ceria-titania. J Phys Chem B 109:1708–1714
28. Fang J, Bi X, Si D, Jiang Z, Huang W (2007) Spectroscopic studies of interfacial structures of CeO_2-TiO_2 mixed oxides. Appl Surf Sci 253:8952–8961
29. Lowell S, Shields JE, Thomas MA, Thommes M (2004) Characterization of porous solids and powders: surface area, pore size and density. Kluwer Academic Publishers, The Netherlands
30. Zhang F, Chan SW, Spanier JE, Apak E, Jin Q, Robinson RD, Herman IP (2002) Cerium oxide nanoparticles: size-selective formation and structure analysis. Appl Phys Lett 80:127–129
31. Tsai SJ, Cheng S (1997) Effect of TiO_2 crystalline structure in photocatalytic degradation of phenolic contaminants. Catal Today 33:227–237
32. Yao HC, Yao YFY (1984) Ceria in automotive exhaust catalysts. I. Oxygen storage. J Catal 86:254–265
33. Hori CE, Ng KYS, Brenner A, Rahmoeller KM, Belton D (2001) The effects of aging temperature and aging time on the oxygen storage capacity of Pt-Rh/$CeZrO_2$ catalysts. Braz J Chem Eng 18(1):23–33
34. Burroughs P, Hamnett A, Orchard AF, Thornton G (1976) Satellite structure in the X-ray photoelectron spectra of some

binary and mixed oxides of lanthanum and cerium. J Chem Soc, Dalton Trans 17:1686–1698
35. Li S, Huaqing Z, Zhangfeng Q, Guofu W, Yagang Z, Zhiwei W, Zhikai L, Gang C, Weiwen D, Zhonghua W, Lirong Z, Jing Z, Tiandou H, Jianguo W (2014) Morphologic effects of nano CeO_2–TiO_2 on the performance of Au/CeO_2–TiO_2 catalysts in low-temperature CO oxidation. Appl Catal B 144:498–506
36. Soria J, Coronado JM, Conesa JC (1996) Spectroscopic study of oxygen adsorption on CeO_2/gamma-Al_2O_3 catalyst supports. J Chem Soc-Faraday Trans 92(9):1619–1626
37. Mamontov E, Egami T, Brezny R, Koranne M, Tyagi S (2000) Lattice defects and oxygen storage capacity of nanocrystalline ceria and ceria-zirconia. J Phys Chem B 104:11110–11116
38. Fornasiero P, Di-Monte R, Ranga-Rao G, Kaspar J, Meriani S, Trovalleri A, Graziani M (1995) Rh-loaded CeO_2-ZrO_2 solid solutions as highly efficient oxygen exchangers: dependence of the reduction behavior and the oxygen storage capacity on the structural properties. J Catal 151:168–177
39. Wang R, Xu H, Liu X, Ge Q, Li W (2006) Role of redox couples of $Rh^0/Rh^{\delta+}$ and Ce^{4+}/Ce^{3+} in CH_4/CO_2 reforming over Rh–CeO_2/Al_2O_3 catalyst. Appl Catal A 305:204–210
40. Vis JC, van't Blik HFJ, Huizinga T, van Grondelle J, Prins R (1985) The morphology of rhodium supported on TiO_2 and Al_2O_3 as studied by temperature-programmed reduction-oxidation and transmission electron microscopy. J Catal 95:333–345
41. Cuauhtémoc, I. Catalizadores de Rh-soportado y su aplicación en la oxidación catalítica en fase Líquida de aditivos contaminantes presentes en la gasolina. PhD thesis, In Spanish. Chemical Department, Universidad Autónoma Metropolitana. http://148.206.53.84/tesiuami/UAMI14203.pdf